

# Direct measurement of Chern numbers in the diffraction pattern of a Fibonacci chain

A. Dareau<sup>1,†</sup>, E. Levy<sup>2,3,†</sup>, M. Bosch Aguilera<sup>1</sup>, R. Bouganne<sup>1</sup>, E. Akkermans<sup>2</sup>, F. Gerbier<sup>1</sup>, and J. Beugnon<sup>1\*</sup>

<sup>†</sup> These authors contributed equally to this work

<sup>1</sup>Laboratoire Kastler Brossel, Collège de France, CNRS,  
ENS-PSL Research University, UPMC-Sorbonne Universités,  
11 Place Marcelin Berthelot, 75005 Paris, France

<sup>2</sup>Department of Physics, Technion Israel Institute of Technology, Haifa 32000, Israel and

<sup>3</sup>Rafael Ltd., P.O. Box 2250, Haifa 32100, Israel

(Dated: June 10, 2022)

Topological properties are now understood to be a key feature of many different physical systems, from topological insulators to quasicrystals. Such properties are often encoded into integer-valued topological invariants, such as winding or Chern numbers, usually related to transport or spectral measurements. We report on an experiment where the Chern numbers of quasicrystalline structures are directly determined by an interferometric approach. We show that all the possible Chern numbers for finite-length Fibonacci chains can be observed directly in their diffraction pattern. Finally, we also demonstrate quantitatively the stability of these topological invariants with respect to structural disorder.

PACS numbers: 41.20.Jb, 61.44.Br, 03.65.Vf, 73.43.Lp, 11.15.Yc

In the last few decades, several concepts issued from topology, a well-established branch of mathematics, have found increasing use in various areas of physics. Topology generalizes the notion of symmetry classes by classifying physical objects into distinct families, or classes, which cannot be related by continuous deformations. A well-known example from geometry is the Gauss classification of surfaces in three-dimensional space by their genus, roughly equivalent to the number of holes piercing them (*e.g.* a doughnut cannot be continuously deformed into a sphere). More generally, topological classes are characterized by one or a set of integer numbers, called topological invariants due to their stability against a broad range of perturbations which may be directly observable. An iconic example from condensed matter physics is the integer quantum Hall effect, where the Hall conductance  $\sigma_H$  of two-dimensional semi-conductors in a strong magnetic field is quantized in integer multiples of a fundamental conductance  $\sigma_0$  [1]. The quantized behavior can be linked to the topological properties of the filled electronic bands in the presence of the applied magnetic field, characterized by a so-called Chern number  $\mathcal{C}$  such that  $\sigma_H = \mathcal{C}\sigma_0$  [2, 3]. Chern numbers and other topological invariants play an important role in many other situations, including the classification of topological defects in symmetry-broken phases [4], quantum anomalies [5], topological insulators and superconductors [6], band structures with Dirac [7] or Weyl points [8, 9], and also quasicrystals.

Quasicrystals (hereafter QC) are structures having some of their physical properties (*e.g.* dielectric coefficient, potential, reflectivity, ...) modulated according to a deterministic but non periodic pattern. Despite their lack of periodicity, QC exhibit long-range order and show sharp diffraction peaks [11, 12]. The discovery of QC opened a new avenue for solid-state physics, material sci-

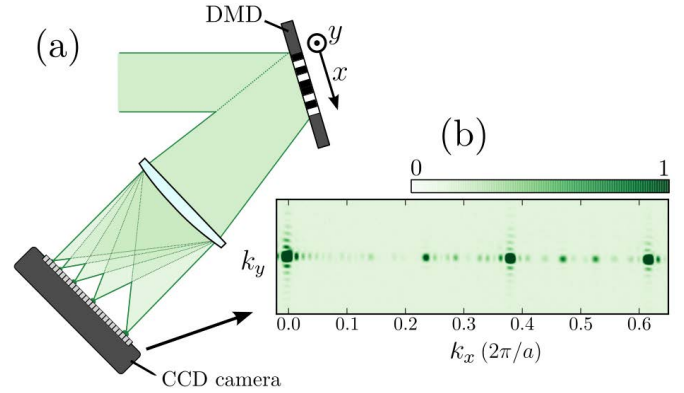


FIG. 1. Experimental setup. (a) Sketch of the optical setup [10]. A collimated laser beam at a wavelength of 532 nm diffracts off a grating programmed on a Digital Mirror Device (DMD). The far-field diffraction pattern is measured on a CCD camera. (b) When the grating is structured following a Fibonacci sequence along the horizontal  $x$  direction (and uniform along the vertical  $y$  direction), we observe diffraction peaks characteristic of the quasiperiodic structure of the chain.

ence and photonics. A well-known example in one space dimension is the Fibonacci chain (denoted as  $S_\infty$ ), *i.e.* an infinitely long one-dimensional structure modulated according to the Fibonacci sequence [13]. The study of propagating waves (acoustic, optical, matter, ...) propagation in these quasiperiodic structures reveals a highly lacunar fractal energy spectrum, with an infinite set of energy gaps [13–15]. Each gap is centered at a location  $k_q = p + q/\tau$  in appropriate units [12], which also corresponds to one of the peaks observable in the diffraction pattern of the structure. Here  $q$  and  $p(q)$  are integers and  $\tau = (1 + \sqrt{5})/2$  is the golden mean.

Structural and transport properties of QC have been

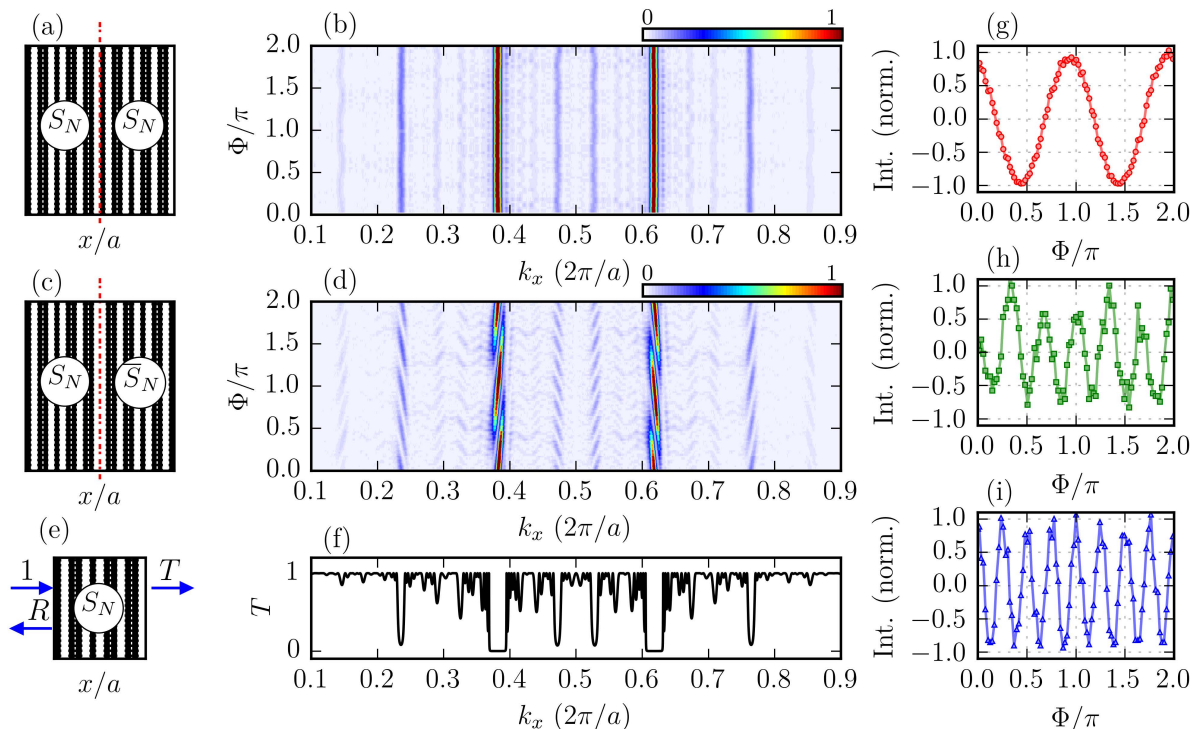


FIG. 2. Influence of the phason degree of freedom on the diffraction pattern of a Fibonacci grating. (a) Structure composed by the juxtaposition of two identical Fibonacci chains along  $x$  (repeated along  $y$ ). White lines correspond to reflecting mirrors (B letters in the Fibonacci chain) and black to non-reflecting mirrors (A letters in the Fibonacci chain). For clarity, this example is shown for a chain of length  $F_6 = 13$ . (b) Measured diffraction pattern for two Fibonacci chains of length  $F_{10} = 89$  as depicted in Fig. 2A. Each line corresponds to the diffraction pattern for a given value of the phason degree of freedom  $\Phi$ . The global pattern is almost independent of  $\Phi$ . (c) Structure composed by the juxtaposition of a Fibonacci chain and of the reversed chain along  $x$  (repeated along  $y$ ). (d) Measured diffraction pattern for the structure depicted in Fig. 2C with a length  $F_{10} = 89$ . (e) Sketch of a transmission experiment. (f) Transmission of a 1D Fibonacci chain (as calculated in [16]). Gaps appear at the same position as the peaks of the diffraction pattern. (g)-(i) Cuts along vertical lines of Fig. 2D for three different values of  $k_x = (2\pi/a) \times (0.618)$  (g),  $0.146$  (h) and  $0.472$  (i) corresponding respectively to Chern numbers  $q = 1, -3, 4$ .

well-studied, especially in 1D. The so-called gap labelling theorem [17], among other works [18], has provided a topological understanding of these properties. This theorem predicts, for the infinite Fibonacci chain  $S_\infty$  (and for a large class of QC), that the integrated density of states  $\mathcal{N}(k_q)$  at wavenumbers  $k_q$  inside a gap takes the simple form

$$\mathcal{N}(k_q) = p + q/\tau. \quad (1)$$

The integers  $q$  are Chern numbers [17, 19–21] and the integers  $p(q)$  keep  $\mathcal{N}(k_q)$  normalized within  $[0, 1]$ . These features have been widely studied [19, 20, 22] and recently revisited [16, 21] in the wake of the growing interest in topological properties of solid-state systems. In a recent work, the gap-labelling theorem was used to identify the experimental gaps observed in the fluorescence spectrum of cavity polaritons in a quasiperiodic setup [15].

In this letter, we show that Chern numbers also characterize a fundamental, purely structural aspect of QC and can be directly measured in their diffraction pattern. We

realized a simple optical setup which allows us to generate any finite-length Fibonacci chain. The corresponding Chern numbers  $-q$  in (1) – appear as winding numbers clearly visible in the diffraction patterns of the Fibonacci chains we studied. Moreover this new approach allowed us to obtain a “topological map” of these chains and to measure, in a simple setup, the Chern numbers associated to each peak. We measured all possible Chern numbers (from  $q = -44$  to  $q = +44$ ) of a structure with 89 elements. Our method provides a new and original experimental approach to study topological properties of matter, different from transport or topological pumping experiments which typically rely on edge states localized on the boundaries [1, 6, 23], and from spectral measurements using cavity polaritons [15, 24] or photonic crystals [25].

In our experiment (see Fig. 1), we realized Fibonacci chains using a Digital Micromirror Device (DMD), *i.e.* an array of about one million micron-sized mirrors (“pixels”) of size  $a \times a$ . Each mirror can be independently

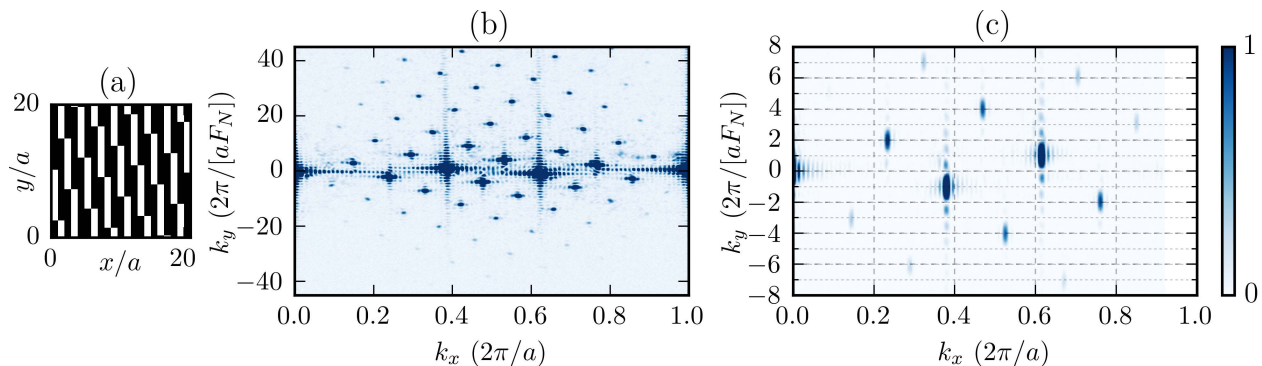


FIG. 3. Two-dimensional map of Chern numbers. (a) Exemplary reflectance of the DMD used for the data presented in this figure. White (resp. black) pixels correspond to reflective (resp. non-reflective) mirrors. The bottom line is the Fibonacci sequence for  $\Phi = 0$ . The other lines correspond to the phase-shifted Fibonacci chains scanning  $\Phi$  from 0 to  $2\pi$ . For clarity, this example is shown for a chain of length  $F_7 = 21$ . (b) Two-dimensional diffraction pattern measured on the camera for a set of 89 phase-shifted chains with  $F_{10} = 89$  letters. The axes are calibrated to directly display the diffraction pattern as a function of  $k_x$  and  $k_y$ . We observe peaks at the same positions along  $k_x$  as in Fig. 2B but shifted along the vertical axis to  $k_y = q \times \left(\frac{2\pi}{aF_N}\right)$ . We observe an asymmetry between the intensity of the diffraction peaks for positive and negative  $k_y$  values. This is not a fundamental property of Fibonacci chains. Rather it is an effect due to the structure of the DMD leading to an asymmetric diffraction envelope. This feature originates from the structure of the micromirrors. (c) Zoom on Fig. 3B.

switched between a reflective ( $B$ ) and a non-reflective ( $A$ ) state. We illuminated the grating with monochromatic light [10], and observed the far-field diffraction pattern on a CCD camera. According to Fourier optics, this pattern is determined by the Fourier transform of the reflectance of the DMD. For a given configuration  $\{x_B\}$  of reflecting pixels, the electric field amplitude in the Fourier plane is given by  $A(k_x) = \sum_B e^{ik_x x_B}$  modulated by an envelope function originating from the DMD structure. The measured light intensity  $I$  is proportional to  $|A(k_x)|^2$ .

We now detail the construction of the configurations  $\{x_B\}$ . It is useful to first review a few properties of finite-length Fibonacci chains  $S_N$ , as opposed to the infinite chain  $S_\infty$  discussed in the introduction. Finite-size chains of given length form a family of one-dimensional quasiperiodic structures, which are all segments of  $S_\infty$ , and which can be deduced from each other by changing a structural degree of freedom termed a *phason* [16]. In this work we generate the  $S_N$  chains using the characteristic function approach. We define a discrete map  $\chi_n$  taking, for each pixel  $n$ , two possible values  $\pm 1$  that we associate to the state of the mirror ( $A = 1, B = -1$ ). Among possible choices [26–28], we consider the form proposed in [29],

$$\chi_n(\Phi) = \text{sign} \left[ \cos(2\pi n \tau^{-1} + \Phi + \Phi_0) - \cos(\pi \tau^{-1}) \right], \quad (2)$$

where we identify the phason  $\Phi$ , which can be safely ignored for  $S_\infty$  but not for its finite segments  $S_N(\Phi) \equiv [\chi_1 \chi_2 \cdots \chi_{F_N}]$  (here  $F_N$  denotes the  $N^{\text{th}}$  Fibonacci number). As shown in [16], for a given structure length  $F_N$ , varying  $\Phi$  over a period  $[0, 2\pi)$  induces a series of  $F_N$  local structural changes occurring one at a time and generat-

ing  $F_N$  non-redundant chains (see Fig. 3A). The value of  $\Phi_0$  in (2) is chosen as  $\Phi_0 = -(F_N + 1)\pi/\tau$  so that the chain  $S_N(0)$  presents a palindromic symmetry (*i.e.* a mirror symmetry with respect to its center).

The topological properties of finite-length QC – *e.g.* the winding of scattering phases [16] or the topological pumping of boundary states, as studied experimentally in [21, 23] – are intimately connected to the phason. A detailed construction based on the “Cut and Project” method is presented in the Supplemental Material [10] where we show that the reciprocal space of the  $(x, \Phi)$  variables has the topology of a torus and the Chern numbers associated to each diffraction peak are winding numbers around the torus. Although the positions of the diffraction peaks and Eq. (1) are only approximate for finite chains, we emphasize that the integer values of the Chern numbers are exact even for finite size segments (see the discussion in [10]). The finite size only results in the existence of an upper limit to the Chern numbers.

As a preliminary experiment, we programmed along the  $x$ -axis a Fibonacci grating of length  $L = F_{10} \times a$ , with  $F_{10} = 89$ . We displayed one-pixel-large vertical lines either in reflective ( $B$ ) or non-reflective ( $A$ ) state according to Eq. (2) (see Fig. 1). We show in Fig. 1B the measured diffraction pattern. Within our experimental resolution, we cannot distinguish the positions of the peaks from  $k_q = p + q/\tau$  (in units of  $2\pi/a$ ), the expected positions for the infinite chain. In the following, we note  $A_0(k_x)$  the diffraction amplitude from this reference chain and  $I_0(k_x)$  the corresponding intensity.

To reveal the topological features hidden in this pattern, we studied the effect of the phason degree of freedom by scanning over all chains corresponding to the

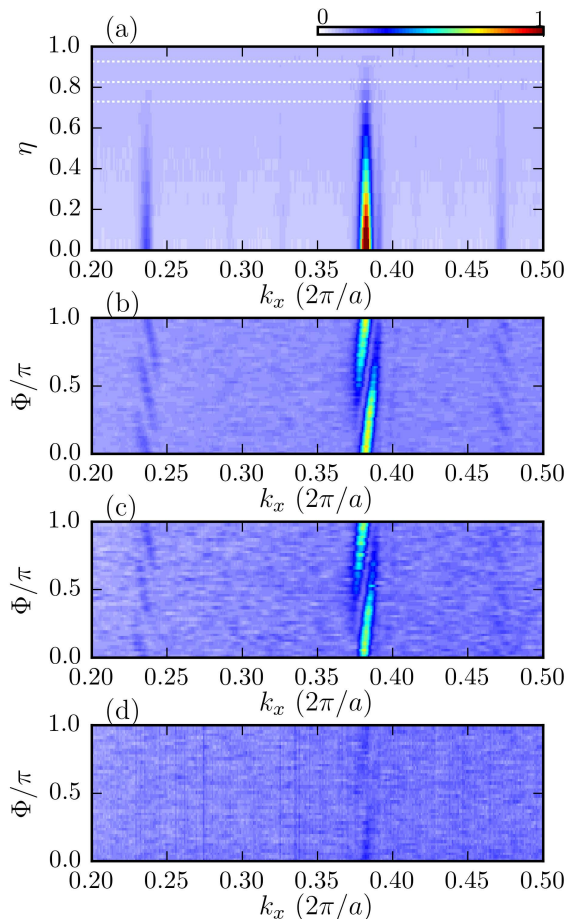


FIG. 4. Robustness of the topological features against structural noise. (a) Diffraction pattern of the Fibonacci and reversed Fibonacci chain at  $\Phi = 0$  and for different levels of noise  $\eta$  (see text). Each line corresponds to a single diffraction pattern. The three white dotted lines correspond to three specific values of  $\eta = 0.73, 0.83$  and  $0.93$  chosen as examples. (b)-(d) Evolution of the diffraction pattern when varying  $\Phi$  for three different noise levels. (b)  $\eta = 0.73$ , (c)  $\eta = 0.83$ , (d)  $\eta = 0.93$ .

$F_N$  distinct and relevant values of  $\Phi$ . In a first experiment, we measured the diffraction pattern of a grating consisting of a Fibonacci chain next to itself (“ $S_N + S_N$ ” configuration) (see Fig. 2A). All the results are consolidated to form the graph shown in Fig. 2B, where each  $\Phi$  value corresponds to a single diffraction measurement. We observe vertical stripes located at a value  $k_q$  corresponding to gaps in the transmission spectrum (Fig. 2F). These stripes are independent of  $\Phi$ . In a second experiment, following [16], we used a grating consisting of a Fibonacci chain next to its mirror image (“ $S_N + \bar{S}_N$ ” configuration) (see Fig. 2C). The resulting diffraction pattern is strikingly different (see Fig. 2D). The vertical stripes are now striated to form a regular and well-structured pattern. The intensities, measured at the original loca-

tion of the diffraction peaks  $k_q$ , vary sinusoidally with  $\Phi$  (Fig. 2G, 2H and 2I), with a period that we identify as  $\pi/|q|$ , *i.e.* inversely proportional to the modulus of the Chern number  $q$  associated to each peak. We also note that the direction of the stripes is determined by the sign of  $q$ .

We explain these observations in terms of a “Young’s double slit” interference between the waves diffracted by the two chains. In both experiments, ( $S_N + S_N$ ) and ( $S_N + \bar{S}_N$ ), the diffracted field is the coherent sum of the amplitude for each chain. Changing  $\Phi$  is equivalent, as discussed in [10], to a translation by a varying distance along the infinite chain  $S_\infty$  and thus to an additional phase factor in the diffracted amplitude. We show in the Supplemental Material [10] that, for a given wavenumber  $k_q$ , the phase shift of the diffracted field with respect to the reference chain is  $q\Phi$ . In the first experiment (“ $S_N + S_N$ ” configuration – Fig. 2A), the diffracted fields for both chains at a diffraction peak  $k_q$  are summed so that the intensity is  $I_{S_N+S_N} = |A_0(k_q)e^{iq\Phi}(1 + e^{-i\phi_s})|^2 = 2I_0(k_q)(1 + \cos(\phi_s))$ , where the phase  $\phi_s = k_q a F_N$  is due to the separation between the two “slits”. The diffraction pattern is thus independent of the phason  $\Phi$ . By contrast, in the second experiment (“ $S_N + \bar{S}_N$ ” configuration – Fig. 2C), the two chains  $S_N$  and  $\bar{S}_N$  are related by a mirror symmetry. As detailed in the Supplemental Material [10], this leads to  $I_{S_N+\bar{S}_N} = |A_0(k_q)e^{iq\Phi}e^{-i\phi_s} + A_0(k_q)e^{-iq\Phi}e^{i\phi_s}|^2$  and the intensity at a diffraction peak is then given by

$$I_{S_N+\bar{S}_N}(k_q, \Phi) = 4I_0(k_q) \cos^2(q\Phi - \phi_s), \quad (3)$$

a sinusoidal function of  $\Phi$  with period  $\pi/|q|$  as observed experimentally[30].

In a third experiment, we used the  $e^{iq\Phi}$  dependence of the diffracted field in a different way which allowed us to obtain a single-shot measurement of all available Chern numbers  $q$ . We programmed each of the  $F_N$  different  $S_N(\Phi)$  chains on horizontal lines along the  $x$ -direction that we piled up along the  $y$  direction, thereby forming an  $F_N \times F_N$  array where the phason degree of freedom is scanned from 0 to  $2\pi$  along the vertical direction  $y$ . The  $y$  direction can then be identified to  $\Phi$  (see Fig. 3A) and the measured diffraction pattern in the  $(k_x, k_y)$  plane is associated to a pattern in the  $(k_x, k_\Phi)$  plane with a normalization of the  $k_y$  axis by  $2\pi/aF_N$ . The diffraction pattern of the  $F_N \times F_N$  array is shown in Fig. 3B and Fig. 3C. It displays a set of discrete peaks at well-defined positions in the  $(k_x, k_\Phi)$  plane. This result follows from our previous analysis, *i.e.* from the  $e^{iq\Phi}$  dependence of the diffracted field. We indeed observe an intensity profile which exhibits peaks located at the values  $k_q$  obtained previously for single chains, but shifted along  $k_\Phi$  by a quantity equal to the Chern number  $q$ . This direct measurement of Chern numbers in a single-shot experiment thereby provides a “topological map” of the Fibonacci chain. For a finite chain of length  $F_N$ , peaks with Chern

numbers  $0 < |q| \leq F_N/2$  are expected [10]. In our experiment having  $F_{10} = 89$ , we observe all the possible values for the Chern numbers.

Finally, in a fourth experiment, we explored the robustness of the diffraction pattern and of its topological features against structural noise. We studied a similar configuration as in the second experiment (“ $S_N + \bar{S}_N$ ”) but introduced noise by randomly selecting a fraction  $\eta$  of the vertical lines ( $0 \leq \eta \leq 1$ ) whose states (reflective or non-reflective) were also chosen at random [10]. Thus,  $\eta = 0$  corresponds to a non-perturbed Fibonacci pattern and  $\eta = 1$  to a random chain. The resulting diffraction pattern is averaged over many realizations of the noise [10]. In Fig. 4A, we show how the diffraction pattern evolves with increasing  $\eta$ . As expected, peaks are washed out when increasing the fraction  $\eta$ . We select in Fig. 4B three specific values of  $\eta$  ( $\eta = 0.73, 0.83$  and  $0.93$ ) and show the evolution of the diffraction pattern when scanning  $\Phi$ . Even for very weak peak signals, the modulation of the peak amplitude is always present and keeps the same frequency and direction. This demonstrates explicitly the expected robustness of the topological properties of the Fibonacci chains captured by the winding with  $\Phi$  of the diffracted field.

In this work we demonstrate a simple way to measure topological invariants associated with quasicrystalline structures. Although we worked with the simplest example, the Fibonacci chain, our method is not limited to it and could be applied to many other quasicrystals. A two-dimensional array of mirrors is also well suited to extend this study to the determination of topological invariants for 2D tilings where much less is known than for 1D structures [31, 32].

A.D. and E.L. contributed equally to this work. We acknowledge financial support from the European Research Council under grant 258521 (MANYBO) and by the Israel Science Foundation under grant 924/09. We thank R. Mosseri for stimulating discussions.

---

\* beugnon@lkb.ens.fr

- [1] K. von Klitzing, Rev. Mod. Phys. **58**, 519 (1986).
- [2] D. J. Thouless, M. Kohmoto, M. P. Nightingale, and M. den Nijs, Phys. Rev. Lett. **49**, 405 (1982).
- [3] J. Avron, D. Osadchy, and R. Seiler, Physics Today **56**, 38 (2003).
- [4] N. D. Mermin, Rev. Mod. Phys. **51**, 591 (1979).
- [5] H. B. Nielsen and M. Ninomiya, Physics Letters B **130**, 389 (1983).
- [6] M. Z. Hasan and C. L. Kane, Rev. Mod. Phys. **82**, 3045 (2010).
- [7] A. H. Castro Neto, F. Guinea, N. M. R. Peres, K. S. Novoselov, and A. K. Geim, Rev. Mod. Phys. **81**, 109 (2009).
- [8] S. Xu, I. Belopolski, N. Alidoust, M. Neupane, G. Bian, C. Zhang, R. Sankar, G. Chang, Z. Yuan, C. Lee, S. Huang, H. Zheng, J. Ma, D. Sanchez, B. Wang, A. Bansil, F. Chou, P. Shibaev, H. Lin, S. Jia, and M. Hasan, Science **349**, 613 (2015).
- [9] L. Lu, Z. Wang, D. Ye, L. Ran, L. Fu, J. D. Joannopoulos, and M. Soljačić, Science **349**, 622 (2015).
- [10] “For details, see Supplemental Materials,”.
- [11] D. Shechtman, I. Blech, D. Gratias, and J. W. Cahn, Phys. Rev. Lett. **53**, 1951 (1984).
- [12] P. Steinhardt and S. Östlund, *Physics of quasicrystals* (World Scientific, 1987).
- [13] M. Kohmoto, B. Sutherland, and K. Iguchi, Phys. Rev. Lett. **58**, 2436 (1987).
- [14] J. M. Luck, Phys. Rev. B **39**, 5834 (1989).
- [15] D. Tanese, E. Gurevich, F. Baboux, T. Jacqmin, A. Lemaître, E. Galopin, I. Sagnes, A. Amo, J. Bloch, and E. Akkermans, Phys. Rev. Lett. **112**, 146404 (2014).
- [16] E. Levy, A. Barak, A. Fisher, and E. Akkermans, arXiv:1509.04028 (2015).
- [17] J. Bellissard, A. Bovier, and J. Ghez, Reviews in Math. Physics **4**, 1 (1992).
- [18] J. Bellissard, B. Iochum, E. Scoppola, and D. Testard, Comm. Math. Phys. **125**, 527 (1989).
- [19] B. Simon, Adv. Appl. Math. **3**, 463 (1982).
- [20] H. Kunz, Phys. Rev. Lett. **57**, 1095 (1986).
- [21] I. Dana, Phys. Rev. B **89**, 205111 (2014).
- [22] D. Damanik and A. Gorodetski, Commun. Math. Phys. **305**, 221 (2011).
- [23] Y. E. Kraus, Y. Lahini, Z. Ringel, M. Verbin, and O. Zeitlinger, Phys. Rev. Lett. **109**, 106402 (2012).
- [24] F. Barboux and et al., in preparation (2016).
- [25] S. A. Skirlo, L. Lu, Y. Igarashi, Q. Yan, J. Joannopoulos, and M. Soljačić, Phys. Rev. Lett. **115**, 253901 (2015).
- [26] H. Kesten, Acta Arith. **12**, 193 (1966).
- [27] S. Ostlund and R. Pandit, Phys. Rev. B **29**, 1394 (1984).
- [28] C. Godreche and J. Oguey, Journal de Physique (France) **51**, 21 (1990).
- [29] Y. E. Kraus and O. Zeitlinger, Phys. Rev. Lett. **109**, 116404 (2012).
- [30] Note that the topological information is thus contained within only half the  $2\pi$ -period of  $\Phi$ .
- [31] Y. E. Kraus, Z. Ringel, and O. Zeitlinger, Phys. Rev. Lett. **111**, 226401 (2013).
- [32] D. T. Tran, A. Dauphin, N. Goldman, and P. Gaspard, Phys. Rev. B **91**, 085125 (2015).
- [33] E. Levy and et al., in preparation (2016).
- [34] A. König and N. D. Mermin, Phys. Rev. B **56**, 13607 (1997).
- [35] A. König and N. D. Mermin, American Journal of Physics **68**, 525 (2000).
- [36] S. Parameswaran, A. Turner, D. Arovas, and A. Vishwanath, Nature Physics **9**, 299 (2013).
- [37] N. de Bruijn, Math. Proc. **A84**, 27 (1981).
- [38] V. Elser, Acta Cryst. **A42**, 36 (1986).
- [39] R. Zia and W. Dallas, Journal of Physics A **18**, L341 (1985).
- [40] R. Mosseri and F. Bailly, Journal de Physique I **2**, 1715 (1992).

## S1-METHODS

### Optical setup

We used a 532 nm laser source to illuminate our Digital Micromirror Device (DMD). The laser output is coupled into an optical fiber used as a spatial mode filter. The fiber output was expanded to obtain a Gaussian beam with  $1/e^2$  radius of about 5 mm, apertured to give a roughly uniform illumination spot with a diameter of about 2.5 mm. This size was chosen empirically to obtain the sharpest observable diffraction peaks. For larger beams the imperfections (in particular, lack of flatness) of the DMD surface become more important and limit the achievable spot sizes.

The DMD (model DLP7000 from *Texas Instruments*) consists of a matrix of  $1024 \times 768$  square micromirrors with a size  $a = 14 \mu\text{m}$ . The angle of incidence of the laser on the DMD surface is on the order of  $22^\circ$  (see Fig. 5). Depending on the mirror state the light is reflected almost perpendicularly to the DMD plane (state B) or to a large angle and then blocked (state A). The diffracted light is focused on a CCD camera using a 2" diameter aspherical lens with a focal of  $f = 100$  mm. The axes of the CCD camera – corresponding to the reciprocal space from the DMD plane – are calibrated by imprinting a periodic lattice of period  $2a$  on the DMD, which gives peaks separated from the zeroth order by  $k_x = \pi/a$ .

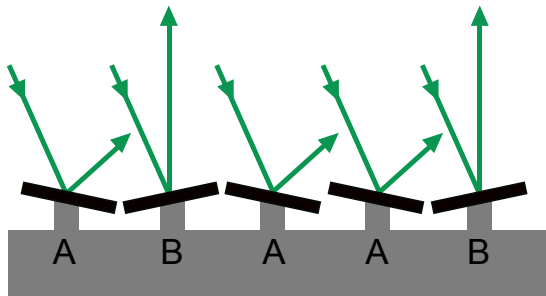


FIG. 5. Sketch of the DMD. Each mirror can be flipped individually between two positions. In position B light is reflected perpendicularly to the DMD and focused on the camera. In position A light is reflected with a larger angle and then blocked far away from the diffraction structure.

### Noise generation

We introduced noise in our DMD pattern in the following way. The initial signal is the Fibonacci chain with its mirrored image (see Fig. 2C in the main text). Noting  $F_N$  the chain length (we used  $F_N = 89$  in our experiments), the total signal has a length of  $2F_N$ . We randomly choose  $N_{\text{noise}}$  mirrors without replacement from the  $2F_N$ -long total chain. The state of the selected mirrors is then ran-

domly chosen between reflective and non-reflective with equiprobability. The resulting one-dimensional chain is then replicated on each line of the DMD, so that the final pattern consists of a collection of vertical lines. This constitutes a single realization of a noisy pattern with a level of noise of  $\eta = N_{\text{noise}}/(2F_N)$ . Note that this algorithm *a priori* generates independent noise for the two parts of the chain (Fibonacci and mirrored Fibonacci).

To average over several realizations of the noise pattern, we reproduced the procedure by randomly choosing a new set of mirrors and randomly flipping them. Each line from the figures 4A to 4D in the main text is obtained by averaging the measured diffraction signal over 200 independent realizations of the noise. In order to speed up the data acquisition process, we dynamically control the DMD so that it scans over all the noise realizations during the CCD camera exposure time, and the average is made while the image is recorded.

## S2-DIFFRACTION AMPLITUDES

We detail here the calculations of the diffraction patterns for various configurations studied in the main text. The Fibonacci chain of length  $F_N$  is defined by  $S_N(\Phi) \equiv [\chi_1 \chi_2 \cdots \chi_{F_N}]$  with the characteristic function given in (2)

As in the main article, we choose  $\Phi_0 = -(F_N + 1)\pi/\tau$ , which is such that  $\Phi = 0$  corresponds to a *palindromic* chain (*i.e.*  $S_N = \bar{S}_N$  with  $\bar{S}_N \equiv [\chi_{F_N} \cdots \chi_1]$ ) [16]. The reflectance  $R_n$  of a vertical line of pixels at position  $x = na$  is given by  $R_n(\Phi) = \frac{1 - \chi_n(\Phi)}{2}$  which is either 0 (pixels A) or 1 (pixels B). The diffracted amplitude is thus proportional to the sum of phase factors over all the B pixels, namely  $\sum_B e^{ik_x x_B(\Phi)}$ .

We first consider a single chain  $S_N(\Phi)$  and a specific wavevector  $k_q$  corresponding to one of the peaks of the diffraction pattern. The complex valued amplitude at this wavevector  $k_q$  reads

$$A_q^{S_N}(\Phi) = \sum_B e^{ik_q x_B(\Phi)} \equiv \mathcal{A}_q^{S_N} e^{i\theta_q(\Phi)} \quad (4)$$

where  $\mathcal{A}_q^{S_N}$  and  $\theta_q(\Phi)$  are real numbers. The inverted structure  $\bar{S}_N$  is obtained by replacing  $x$  by  $-x + aF_N$  ( $a$  being the pixel size). We thus obtain the corresponding diffraction amplitude as

$$A_q^{\bar{S}_N}(\Phi) = \sum_B e^{ik_q(aF_N - x_B(\Phi))} = \mathcal{A}_q^{S_N} e^{-i\theta_q(\Phi)} e^{ik_q a F_N}. \quad (5)$$

We now take advantage of two results. First, the diffraction intensities at  $k = k_q$  for the two structures  $S_N$  and  $\bar{S}_N$  are the same, and are independent of  $\Phi$ ,  $|A_q^{S_N}(\Phi)|^2 = |A_q^{\bar{S}_N}(\Phi)|^2 = (\mathcal{A}_q^{S_N})^2$ . Second we note that, for a palindromic chain, the diffraction amplitudes are

the same and hence we have  $A_q^{S_N}(0) = A_q^{\bar{S}_N}(0)$  leading to  $k_q a F_N = 2\theta_q(0)$ .

We now proceed to describe the experiment “ $S_N + S_N$ ”. Defining the spatial origin at the center, we obtain

$$A_q^{S_N+S_N}(\Phi) = \mathcal{A}_q^{S_N} e^{i\theta_q(\Phi)} (e^{-2i\theta_q(0)} + 1). \quad (6)$$

As in the case of single chains, the diffraction intensities are identical for the structure and its reverse “ $\bar{S}_N + \bar{S}_N$ ”, and independent of  $\Phi$ :  $|A_q^{S_N+S_N}(\Phi)|^2 = 2(\mathcal{A}_q^{S_N})^2(1 + \cos(2\theta_q(0)))$ .

Finally, we consider the experiment “ $S_N + \bar{S}_N$ ”. We obtain

$$A_q^{S_N+\bar{S}_N}(\Phi) = \mathcal{A}_q^{S_N} \left( e^{i[\theta_q(\Phi)-2\theta_q(0)]} + e^{-i[\theta_q(\Phi)-2\theta_q(0)]} \right). \quad (7)$$

Unlike Eq.(6), the diffraction intensity  $2(\mathcal{A}_q^{S_N})^2(1 + \cos(2\theta_q(\Phi) - 4\theta_q(0)))$  depends sinusoidally on  $\theta_q(\Phi)$ . In the next section we show that  $\theta_q(\Phi)$  is a linear function of  $\Phi$ . The diffraction intensity then depends sinusoidally on  $\Phi$  as observed experimentally.

### S3-THE PHASE TERM $\theta_q(\Phi)$

Here, we wish to show that the phase term  $\theta_q(\Phi)$  in the diffraction amplitude of Eq. (4) is linear with  $\Phi$ , with a slope equal to the Chern number  $q$ . A thorough proof will be given elsewhere [33]. Figure 6 shows how the phase  $\theta_q(\Phi)$  of the diffraction amplitude varies as a function of  $\Phi$  for different values of the wavevector  $k_q$  (equivalently, of the Chern number  $q$ ). The total diffraction phase  $\theta_q(\Phi)$  is a staircase following a linear function of  $\Phi$  with a slope  $q$ . Two more features are worth noting:

1. For a given value of  $q$  (i.e. of  $k_q$ ), the phases of  $S_N$  and  $\bar{S}_N$  are deduced from each other by changing  $\Phi$  into  $-\Phi$  (see Fig. 6).
2. Changing  $k_q$  into  $k_{-q}$  is equivalent to changing  $\Phi$  into  $-\Phi$ .

These results seem to be a rather general feature of the diffraction pattern of both periodic and quasiperiodic structures (see for instance, for a generic discussion not restricted to 1D, [34–36]).

This linear dependence can be understood from a simple calculation. From the characteristic function  $\chi_n$  in Eq. (2), we note that changing  $\Phi$  from an initial value  $\Phi_i$  by an amount  $\Delta\Phi$  is equivalent to a spatial translation along the chain. Specifically, for  $\Delta\Phi = 2\pi/\tau$ , the resultant structure is translated by one pixel, and therefore the diffraction amplitude  $A_q^{S_N}(\Phi_i + 2\pi/\tau)$  carries an additional phase,  $\theta_q(\Phi_i + 2\pi/\tau) = \theta_q(\Phi_i) + ak_q$ . Using the approximation  $k_q = (2\pi/a)(p + q\tau^{-1})$ , leads to  $\theta_q(\Phi_i + 2\pi/\tau) = \theta_q(\Phi_i) + 2\pi q\tau^{-1} = \theta_q(\Phi_i) + q\Delta\Phi$ . As a variation of  $\Phi$  by  $2\pi$  corresponds to  $F_N$  structural

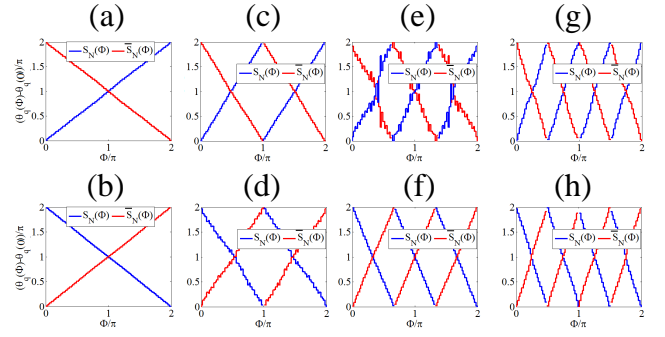


FIG. 6. A numerical plot of the phase  $\theta_q(\Phi)$  of the diffraction amplitude, as a function of  $\Phi$  for the structures  $S_N$  (in blue) and  $\bar{S}_N$  (in red) and for the diffraction peaks  $k_q$  for various  $q$ . (a)-(b)  $q = \pm 1$ , respectively. (c)-(d)  $q = \pm 2$ , respectively. (e)-(f)  $q = \pm 3$ , respectively. (g)-(h)  $q = \pm 4$ , respectively.

changes (see Fig. 7c), then the shift  $\Delta\Phi = 2\pi/\tau$  is associated with  $F_N/\tau$  structural changes. Since each structural change amounts to translate a single “B” pixel by one pixel, each change contributes to  $q\Delta\Phi/(F_N/\tau) = 2\pi q/F_N$  to the additional phase in a staircase, which completes  $q$  periods in one period of  $\Phi$ . We thus write the general phase term as a function of the modulation phase as

$$\theta_q(\Phi_i + \Delta\Phi) = \theta_q(\Phi_i) + q\Delta\Phi. \quad (8)$$

### S4-CHERN NUMBERS - STRUCTURAL ORIGIN

The purpose of this section is to provide a theoretical description of the experiment reported in Fig. 3 of the main article, *i.e.* to obtain the  $(k_x, k_y)$  map. We first recall in subsection basic results of the well-known “Cut and Project” construction of 1D quasicrystals, as well as recent results obtained in [16] that will be useful for the following. Then, in subsection , we describe the global properties of the set  $\{S_N(\Phi)\}$  of all possible Fibonacci chains of length  $F_N$ . This set corresponds to the pattern programmed on the DMD, and possesses specific geometrical and topological properties that we unveil. Finally, using these properties, we explain in subsection the observed diffraction pattern and describe it in terms of Chern numbers.

#### Finite-size Fibonacci chains. Role of the phason

The “Cut and Project” (C&P) method generates a quasiperiodic chain from a primitive  $\mathbb{Z}^2$ -lattice cut by a line  $\Delta$  defined by  $v = u \tan \theta + \text{const}$  (see Fig. 7a). We denote by  $\Delta_\perp$  the direction perpendicular to  $\Delta$  and

define an acceptance window as a band of width  $\Omega$  centered at  $\Delta$ . This realizes the “cut”. A C&P set is obtained by projecting the  $\mathbb{Z}^2$  points inside  $\Omega$  on  $\Delta$  and along  $\Delta_{\perp}$ . There are only two possible distances along  $\Delta$  between neighboring projections, denoted  $\{A, B\}$ . One can generate the infinite Fibonacci chain  $S_{\infty}$  by choosing  $\tan \theta = \tau^{-1}$ ,  $\tau$  being the golden mean. The choice of an origin on  $\Delta$  is irrelevant for the infinite chain  $S_{\infty}$ , but not for finite chains  $S_N$  of length  $F_N$ : the origin fixes the first letter and the iteration of the sequence. We note that C&P and characteristic function methods, as used in the main text, are related through the constant term in the equation for  $\Delta$ , namely  $v = u \tan \theta - \frac{\Phi}{2\pi}$ .

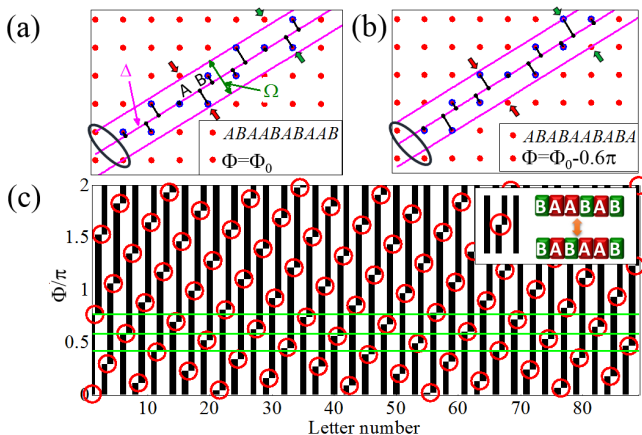


FIG. 7. Phason driving in the Cut & Project method for the slope  $\tau^{-1}$ . (a)-(b) The C&P method for the  $\Phi$  values  $\Phi_0$  and  $\Phi_0 - 0.6\pi$ . An ellipse indicates the origin of the chain. The 10 first letters of the resulting sequences are in the insets. Shifting the band  $\Omega$  along the vertical axis induces two structural changes corresponding to points entering and leaving  $\Omega$  (red/green arrows). (c) Structural color plot. Black(white) regions describe  $B(A)$  letters. Identical structural changes (red circles, inset) occur when scanning  $\Phi$  (e.g. green lines).

The C&P method allows to interpret the  $2\pi$ -periodic, structural degree of freedom  $\Phi$  as the parameter driving the rearrangement of letters along the Fibonacci chain (see Fig. 7). For a chain of length  $F_N$ , each value of  $\Phi$  generates a different segment of  $S_{\infty}$ , and corresponds to some translation along  $\Delta$ . Monitoring the phason  $\Phi$  induces a series of  $F_N$  identical local structural changes equivalent to the inversion of a single 6-letter string  $BAABAB \leftrightarrow BABAAB$ . These changes occur one at a time and are distributed according to a geometrical pattern (see Fig. 7c). The  $\Phi$ -axis, corresponding to the phason direction, is infinite. However, since  $\Phi$  is  $2\pi$ -periodic, the structural information in the phason direction is contained in a single period.

To generate a *finite* chain  $S_N$  of  $F_N$  letters, the slope of the cut  $\Delta$  defined by  $\tan \theta$  must not necessarily be taken as an irrational number, but may be given by a rational approximant  $p/q$  (as long as the unit cell of the

resultant periodic chain remains larger than  $F_N$ ). For the “standard” Fibonacci chain of length 89 (obtained for instance with the substitution rule)  $S_{10}(\Phi_{\text{std}})$ , the approximant has to be at least as good as  $34/55$ . Similarly, to generate the complete set of  $F_N$  finite chains,  $S_N(\Phi)$ , the slope can again be taken as another rational approximant  $p/q$  (provided the unit cell of the resulting periodic pattern is larger than  $2F_N + 1$ ). For the set  $\{S_{10}(\Phi)\}$  the approximant with the smallest possible  $p$  is  $89/144$ .

The C&P method also allows to obtain the Bragg peak structure of  $S_{\infty}$  [37–39]. In the case of a finite segment  $S_N$ , we have observed experimentally that there still exist diffraction peaks, located at approximate values of the exact Bragg peaks spatial frequencies, and also that we were able to probe their topological properties by scanning through the  $F_N$  possible realizations (see Fig. 2 in the main text).

### Properties of the 2D set of Fibonacci chains $\{S_N(\Phi)\}$

We now consider the pattern described in Fig. 7c that is programmed on the DMD and whose diffraction pattern is the topological map of Fig. 3 in the main text. This finite 2D structure may be described as another  $\mathbb{Z}^2$ -lattice rotated by an angle  $\varphi$  with respect to the  $(x, \Phi)$  axes (see Fig. 8a).

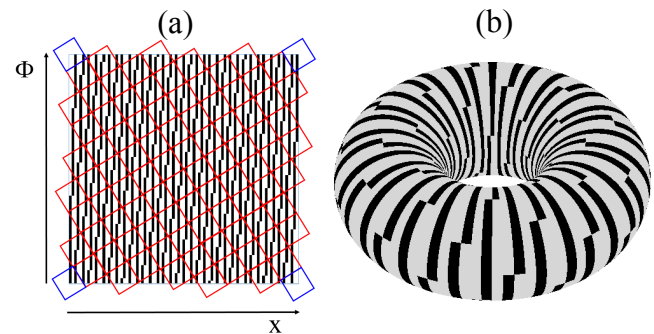


FIG. 8. Structural properties of the 2D set  $\{S_N(\Phi)\}$  for  $N = 10$ . (a) The  $\{S_N(\Phi)\}$  structural  $x$ - $\Phi$  map created through the Cut & Project method (see Fig. 7c) forms a tilted 2D crystal with a unit cell indicated by red and blue squares. This map is a torus obtained by wrapping the map along both axes, so that the four blue squares coincide. (b) An illustration of the resulting torus.

Disregarding the form factor of the 2D unit cell of this structure, the remaining square lattice of points is represented by the function,

$$Q(x, \Phi) = \frac{1}{4\pi^2} \sum_{k,l} \delta(x - k \cos \varphi - l \sin \varphi) \times \delta(\Phi + k \sin \varphi - l \cos \varphi), \quad (9)$$

where the sum is over a finite set of integers  $(k, l)$ . The Fourier transform (disregarding the effect of the finite size of the system on the peaks width) of the rotated  $(x, \Phi)$   $\mathbb{Z}^2$ -lattice is also a  $\mathbb{Z}^2$ -lattice rotated with the angle  $\varphi$  with respect to the reciprocal space  $(k_x, k_\Phi)$ , and represented by,

$$F(k_x, k_\Phi) = \sum_{n,m} \delta(k_x - m \cos \varphi + n \sin \varphi) \times \delta(k_\Phi - m \sin \varphi - n \cos \varphi), \quad (10)$$

where the sum is over an infinite set of integers  $(m, n)$ . It is important to note that the rotation angle  $\varphi$  is not given, for finite chains, by  $\tan \varphi = \tau^{-1}$ . For the set  $\{S_N(\Phi)\}$  generated as discussed previously, the tiling angle of this new  $\mathbb{Z}^2$ -lattice has always a fixed rational slope

$$\tan \varphi = \frac{p_N}{q_N}, \quad (11)$$

where the two mutually prime integers  $(p_N, q_N)$  depend only on  $F_N$  [33]. For  $S_{10}$ , we have  $p_N = 5$  and  $q_N = 8$ .

The  $2\pi$ -periodicity of the set  $\{S_N(\Phi)\}$  in the phason direction  $\Phi$ , together with the fixed rational angle of rotation  $\varphi$ , means that the set may be folded to form a perfect torus (see Fig. 8b).

### Diffraction pattern in terms of Chern numbers

We now discuss the diffraction pattern of the 2D structure of Fig. 7 to obtain both the (approximate)  $k$  values of the Bragg peaks and the corresponding observable (exact) Chern numbers.

The infinite reciprocal space of the finite set  $\{S_N(\Phi)\}$  may be characterized by a finite quasi-Brillouin zone, QBZ $_N$ , (also a torus) which generalizes the usual notion of Brillouin zone. We use the fact that the rotation angle of the  $\mathbb{Z}^2$  reciprocal lattice with respect to the  $(k_x, k_\Phi)$  axes is still described by  $\tan \varphi$  (see Fig. 9).

To build the torus QBZ $_N$  in the  $(k_x, k_\Phi)$  reciprocal space, we set an origin  $(k_x, k_\Phi) = (0, 0)$  at some point and label them with the lattice coordinates  $[m = 0, n = 0]$ . The next step is to identify the three other corners of the QBZ $_N$ , using Eq. (11), to be  $[m = q_N, n = -p_N]$  where  $(k_x, k_\Phi) = (q_N \cos \varphi + p_N \sin \varphi, 0)$ ,  $[m = p_N, n = q_N]$  where  $(k_x, k_\Phi) = (0, p_N \sin \varphi + q_N \cos \varphi)$ , and  $[m = q_N + p_N, n = q_N - p_N]$  where  $(k_x, k_\Phi) = (p_N \sin \varphi + q_N \cos \varphi, p_N \sin \varphi + q_N \cos \varphi)$ . These four points define the torus QBZ $_N$  as represented on Fig. 9. It exactly encloses  $F_N$  points.

We now discuss the normalization of the reciprocal space torus coordinates. The  $k_x$  coordinates may be normalized by  $(p_N \sin \varphi + q_N \cos \varphi)^{-1} = 1/\sqrt{p_N^2 + q_N^2}$  so that  $k_x \in [0, 1]$ . After this normalization, the  $F_N$  points at which  $F(k_x, k_\Phi) \neq 0$  correspond to all possible (approximate) Bragg peaks values  $k_q$ . As for normalization along the  $\Phi$ -axis, it is obtained from the reciprocal

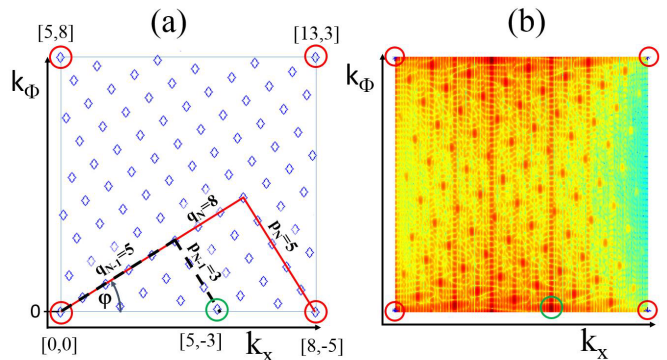


FIG. 9. Construction of the torus QBZ $_N$  for  $N = 10$  with the corresponding values  $p_N = 5$  and  $q_N = 8$ . The red circles define the corners of the torus QBZ $_N$  which encloses  $F_{10} = 89$  points (lattice coordinates  $[m, n]$  are given). The fundamental  $k_\Phi$  value,  $\delta k_\Phi$  corresponding to Chern number equal to 1, is represented by the green circle. This lowest non zero value of  $k_\Phi$  is obtained using the previous approximant  $(p_{N-1}, q_{N-1})$  in the Farey series. (a) An emulated lattice angled at  $\varphi$  (to set notations). (b) The actual 2D Fourier transform of  $\{S_N(\Phi)\}$  for  $N = 10$ .

lattice point  $(\delta k_x, \delta k_\Phi)$  with  $\delta k_\Phi$  the smallest nonzero value of  $k_\Phi$ . The (toroidal) vector between the origin and this lattice point is instrumental to find all points within the QBZ $_N$  torus, namely through the recurrent addition (and winding) of this vector (see Fig. 9). This single fundamental lattice point is defined by  $[m = q_{N-1}, n = -p_{N-1}]$ , where  $p_{N-1}$  and  $q_{N-1}$  are obtained using the preceding approximant of the slope  $\tan \varphi = p_N/q_N$  in the Farey sequence [33],

$$\frac{1}{1} : \frac{1}{1} : \frac{1}{2} : \frac{2}{3} : \frac{3}{5} : \frac{5}{8} : \dots : \frac{p_j}{q_j} : \dots \quad (12)$$

In reciprocal space coordinates, we have

$$(\delta k_x, \delta k_\Phi) = \left( \frac{q_{N-1} \cos \varphi + p_{N-1} \sin \varphi}{\sqrt{p_N^2 + q_N^2}}, q_{N-1} \sin \varphi - p_{N-1} \cos \varphi \right). \quad (13)$$

The expression of  $(\delta k_x, \delta k_\Phi)$  corresponds to the numbering method developed in [40] and we use it to set the  $k_\Phi$ -scales in the reciprocal lattice. The normalized  $k_\Phi$  coordinates correspond to the integer (Chern) numbers

$$C(n, m) \equiv \frac{k_\Phi}{\delta k_\Phi} = \frac{m \sin \varphi + n \cos \varphi}{q_{N-1} \sin \varphi - p_{N-1} \cos \varphi} = mp_N + nq_N \quad (14)$$

These Chern numbers describe how many times the phase of the diffraction amplitude winds around the torus when scanning over a period in the  $k_\Phi$  direction. The last equality is obtained by noting that successive approximants in the Farey series in Eq. (12) fulfill  $|p_{N-1}q_N - q_{N-1}p_N| = 1$ .

The Fourier transform in Eq. (10) can be rewritten in terms of the Chern numbers  $C$  and of the (approximate) Bragg peak values  $k_x$  as,

$$F(k_x, C) = \sum_{n,m} \delta \left( k_x - \frac{m \cos \varphi - n \sin \varphi}{\sqrt{p_N^2 + q_N^2}} \right) \times \delta(C - mp_N - nq_N) \quad (15)$$

where the integers  $(n, m)$  run over the torus  $\text{QBZ}_N$  now entirely defined by

$$\begin{aligned} k_x(m, n) &= (mq_N - np_N) / (p_N^2 + q_N^2) \\ C(m, n) &= mp_N + nq_N \end{aligned} \quad (16)$$

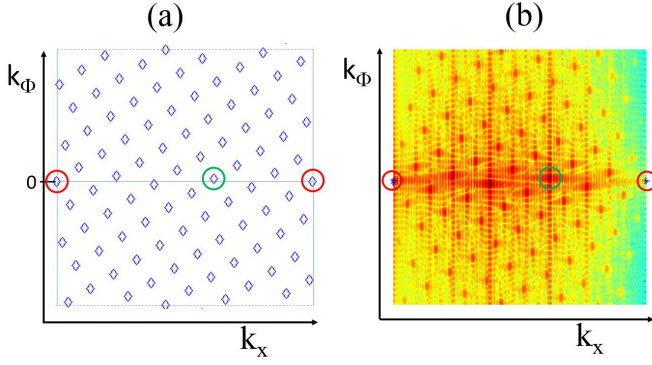


FIG. 10. A properly unwrapped torus  $\text{QBZ}_N$  for  $N = 10$ . The red circles define the 4 corners of the torus  $\text{QBZ}_N$  of Fig. 9. The fundamental  $k_\Phi$  value,  $\delta k_\Phi$  corresponding to Chern number equal to 1, is represented by the green circle.  $k_\Phi$  values now come in pairs of equal magnitude and opposite sign. (a) An emulated lattice angled at  $\varphi$ . (b) The actual 2D Fourier transform of  $\{S_N(\Phi)\}$  for  $N = 10$ .

Additionally, a change of origin can be performed in the  $k_\Phi$  toroidal dimension, such that all reciprocal lattice points with  $F_N/2 \leq k_\Phi/\delta k_\Phi$  are wrapped around the torus to have  $k_\Phi/\delta k_\Phi \rightarrow F_N/2 - k_\Phi/\delta k_\Phi$ . The total number of points in the 2D torus  $\text{QBZ}_N$  is the number of Chern integers available for a given  $N$ . It is given by  $F_N$  and we have  $|C(m, n)| \leq F_N/2$ .

Finally, we note that Chern numbers always appear in pairs of opposite sign associated to the structure length  $F_N$  and its minimal Farey approximate  $\tan(\theta) = p/q$ . For the lowest approximant (periodic system), the values  $C = \pm 1$  will show up first, followed by higher paired values while increasing the ratio  $p/q$ . It is worth noting again that while the Chern numbers  $C(m, n)$  are always integers, the (approximate) Bragg vectors  $k_x(m, n)$  depend on the chain length but they rapidly converge to the exact Bragg value obtained for  $N \rightarrow \infty$ .